AD_____

Award Number: W81XWH-04-1-0323

TITLE: Task-Specific Optimization of Mammographic Systems

PRINCIPAL INVESTIGATOR: Robert Saunders, M.A.

CONTRACTING ORGANIZATION: Duke University
Durham, NC 27705

REPORT DATE: March 2006

TYPE OF REPORT: Annual Summary

PREPARED FOR: U.S. Army Medical Research and Materiel Command
Fort Detrick, Maryland 21702-5012

REPORT DOCUMENTATION PAGE

Form Approved
OMB No. 0704-0188

1. REPORT DATE *(DD-MM-YYYY)*	**2. REPORT TYPE**	**3. DATES COVERED** *(From - To)*
01-03-2006	Annual Summary	15 Feb 2005 - 14 Feb 2006

4. TITLE AND SUBTITLE
Task-Specific Optimization of Mammographic Systems

5a. CONTRACT NUMBER

5b. GRANT NUMBER
W81XWH-04-1-0323

5c. PROGRAM ELEMENT NUMBER

6. AUTHOR(S)
Robert Saunders, M.A.

E-mail: rss@duke.edu

5d. PROJECT NUMBER

5e. TASK NUMBER

5f. WORK UNIT NUMBER

7. PERFORMING ORGANIZATION NAME(S) AND ADDRESS(ES)

Duke University
Durham, NC 27705

8. PERFORMING ORGANIZATION REPORT NUMBER

9. SPONSORING / MONITORING AGENCY NAME(S) AND ADDRESS(ES)
U.S. Army Medical Research and Materiel Command
Fort Detrick, Maryland 21702-5012

10. SPONSOR/MONITOR'S ACRONYM(S)

11. SPONSOR/MONITOR'S REPORT NUMBER(S)

12. DISTRIBUTION / AVAILABILITY STATEMENT
Approved for Public Release; Distribution Unlimited

13. SUPPLEMENTARY NOTES

14. ABSTRACT

During this past year, our research has focused on three objectives. The first objective was to develop a model of scattered radiation in mammographic imaging. This was done to understand how scatter affects image quality by degrading resolution and noise. The second aim continued research that used observer models to understand how resolution and noise affect breast lesion detection and discrimination. The third objective was to conduct an observer experiment with several mammographers to examine how reduced dose and different medical displays affect lesion detection and discrimination. For future work, we will analyze the data from these experiments to understand how resolution and noise separately and jointly affect cancer detection.

15. SUBJECT TERMS
X-ray Imaging, Digital Imaging

16. SECURITY CLASSIFICATION OF:			**17. LIMITATION OF ABSTRACT**	**18. NUMBER OF PAGES**	**19a. NAME OF RESPONSIBLE PERSON**
					USAMRMC
a. REPORT	**b. ABSTRACT**	**c. THIS PAGE**			**19b. TELEPHONE NUMBER** *(include area code)*
U	U	U	UU	31	

Standard Form 298 (Rev. 8-98)
Prescribed by ANSI Std. Z39.18

Table of Contents

Introduction

The primary screening tool for breast cancer is x-ray mammography. While mammography reduces breast cancer mortality, it has areas for improvement as it misses many early-stage cancers. This research seeks to improve the efficacy of mammography by optimizing the entire image chain for the detection of breast masses and microcalcifications. This research can be split into two stages. The first stage measures the imaging chain's physical characteristics. These characteristics include resolution and noise measurements of x-ray detectors and medical displays. To better understand this physics, this research also has developed models of scattered radiation, as scatter is another major factor affecting resolution and noise. This physical data is then applied in the second research stage. The second stage modifies the resolution and noise of mammographic images. These images are viewed by a combination of observer models and human observers to discover how image quality affects lesion detection and discrimination. This observer data will help guide future optimization of mammographic systems.

Body

This section reviews the progress of the research in addressing the approved statement of work. We have written the sections of the statement of work addressed in last year's annual report in a gray font. We have italicized those parts of the statement of work addressed by our work over the past year. Sections not included in this report are part of our future work.

Task 1: Create a simulation procedure for the anatomical background of mammographic images

- 1.1 Acquire normal mammograms obtained on digital systems for analysis
- 1.2 Categorize the images into the four types of breast composition, as identified by the BIRADS system.
- 1.3 Analyze the geometrical features of these breasts and characterize them with a fixed number of scalar parameters, such as size.
- 1.4 Obtain mammograms from the Digital Database for Screening Mammography (DDSM) to analyze lesion characteristics
- 1.5 Analyze the features of specific lesion types
- 1.6 Create a program that can create images with breast anatomy and breast lesions that allows for user input of specific scalar parameters, such as size.
- 1.7 Establish mapping technique to determine grayscale values of image using sigmoid curve transformation.

Task 2: Calibrate a computational observer (observer model) to emulate the detection task performed by mammographers.

- *2.1 Create a set of anatomical images with the four different background types and different lesions types using the above simulation routine.*
  We had previously acquired a set of normal mammograms that contained images with each of the four different background types, ranging from extremely dense to almost entirely fat-replaced. Using this set of normal mammograms, we inserted simulated lesions using our lesion simulation routine[1,2] to create a large image set with three different types of lesions, benign masses, malignant masses, and malignant microcalcifications.

2.2 Modify the resolution and noise of the images to that consistent with various digital systems.

Using our verified noise modification routine,[3] we simulated the effects of imaging with reduced dose. We created images with noise characteristics emulating three dose levels—full clinical dose, half dose, and quarter dose. We altered the resolution of the images by displaying the images on three different medical displays. These displays included an LCD, a normal CRT, and a CRT with degraded resolution.

2.3 Perform an observer performance experiment with five mammographers.

Five experienced mammographers viewed the image set on three displays using a custom graphical interface. This interface allowed the mammographers to rate the images as containing no lesion, a benign mass, a malignant mass, or microcalcifications.

2.4 Analyze the data from that experiment with Receiver Operating Characteristic Analysis.

Receiver Operating Characteristic Analysis significantly slows down an observer experiment because of the detailed ratings it requires. It also differs from the clinical paradigm by requiring radiologists to specify their confidence in a given decision. In the clinic, radiologists generally make binary decisions as to whether a lesion is present or not. Therefore, this experiment did not use Receiver Operating Characteristic Analysis, but rather used a new categorical rating paradigm that minimized reading time and more closely emulated clinical decision making.

We are currently analyzing the observer data to find overall classification accuracy at different dose levels and on different displays. As well, the data will be analyzed for performance at specific clinical tasks, such as the detection of microcalcifications and discrimination of benign and malignant masses. While currently resolution and noise are considered separately, future work will consider how these two effects jointly affect lesion detection and discrimination.

2.5 Use several computational observers to examine the image set.

We found that this image set was not appropriate for observer model calculations as it did not model resolution, but rather used displays for resolution modification. Therefore, we combined this step with specific aim 3.3, which analyzed images with different simulated noise and resolution characteristics.

Task 3: Create an empirical model that relates the resolution and noise of a digital mammographic system to the detectability of breast lesions.

3.1 Compile a list of MTFs and NPS for commercial radiographic systems, including image processing algorithms and displays.

In last year's progress report, we described our work that measured the physical performance of a clinical prototype digital mammographic detector. We have extended this work this year by conducting a study that

measured the resolution and noise of five medical displays. Please refer to Appendix I for the details of this study.

3.2 *Create a set of 1500 simulated anatomical images with added masses and microcalcifications. The resolution and noise of these images will be modified according to the various configurations collected above.*
An image set was created using similar methods as the one created under specific aim 2.1. In this case, an image set was created that had three different resolution levels, divided among images with resolution corresponding to an LCD, a normal CRT, and a degraded CRT, and three different noise levels according to the level of noise at full dose, half dose, and quarter dose. The noise of the images had been modified according to the previously measured NPS of a digital mammographic detector and the relationship between dose and noise magnitude.[4] The resolution of the images was modified according to the measured resolution of the medical display devices using a previously verified routine.[3,5]

3.3 *Use the observer model to examine each image and determine the detectability of masses or calcifications in each resolution and noise configuration.*
Three different observer models (Non-Prewhitening Matched Filter with Eye Filter (NPWE) observer, the JNDMetrix Visual Discrimination Model, and a Channelized Hotelling Observer (CHO) with Gabor channels) viewed all of the images in this set to determine the detectability of benign masses, malignant masses, and microcalcifications at each noise/resolution configuration. In addition, we examined the impact of resolution and noise on the discriminability between benign and malignant masses.

3.4 *Develop a fitting method for MTF and NPS curves that reduces the curves to scalar parameters*
After obtaining the resolution and noise characteristics, we fit each of them with a multi-parameter exponential function. This provided us with a functional form for the resolution and noise data, which was used by the resolution and noise modification routines.

Task 5: Utilize the empirical model to examine the effect of dose on the detection of microcalcifications and masses and determine the minimum allowable dose level for "safe" mammographic imaging.

5.1 Determine the relationship between dose and noise amplitude for the three specific digital mammographic systems through published measurements.

5.2 *Determine the effect of scatter utilizing previously published models.*
Our previous annual report described our work on scatter using previously published models. Previously published models generally characterize scatter in terms of its magnitude (scatter fraction or scatter to primary ratio). This characterization was appropriate for film-screen systems where scatter primarily affected the contrast of subtle lesions. However, digital systems can overcome these contrast effects, but are still subject to

scatter's resolution and noise effects. Therefore, we created a Monte Carlo model of a digital mammographic detector in order to understand scatter's effects. This model is discussed in more detail in Appendix II.

5.3 Using the previously developed empirical model to analyze the effect of dose on the detectability of masses and microcalcifications.
Last year's annual report discussed research we had conducted using observer models to analyze the effect of dose on lesion detectability. We have furthered that work by conducting a large observer experiment with five mammographers. This observer experiment looked at lesion detection and discrimination under three different dose levels. We are analyzing the results of that experiment.

Task 6: Apply the empirical model to ascertain the effect of a specific image processing algorithms, unsharp masking, on lesion detection and optimize its utilization.

6.1 Examine the clinical parameters used for unsharp masking.

Task 7: Employ the model to examine the influence of two specific display characteristics, display magnification and display resolution, on lesion detection and thus develop guidelines for optimized viewing of digital mammograms.

7.2 Determine the resolution and noise for four display devices, three common Cathode Ray Tube (CRT) devices and one Liquid Crystal Display (LCD) device.
As noted earlier in the response to section 3.1 of the statement of work, we measured the resolution and noise of five medical displays, including three LCDs and two CRTs. In the past two years, LCDs have become more common for medical display. This prompted us to place more emphasis on LCDs than was originally envisioned in the statement of work. Please refer to Appendix I for the details of this display assessment, which was reported in the peer-reviewed literature.

7.3 Fit the resolution and noise properties of the combined display and detector system using the generalized curve-fitting algorithm.

7.4 Input the above into the empirical model in order to develop guidelines for optimized display of mammographic images.

Key Research Accomplishments

- Conducted observer experiment with five mammographers examining the impact of reduced dose on lesion detection and discrimination. This experiment also examined the effect of different medical displays on lesion detection and discrimination.

- Developed Monte Carlo model of digital mammographic system to characterize the effects of x-ray scatter on resolution and noise.

- Created large image set with noise properties emulating mammograms acquired at a reduced dose and emulating resolution of images displayed on different commercial medical displays.

Reportable Outcomes

Presentations

R.S. Saunders and E. Samei, “A Monte Carlo Investigation on the Impact of Scattered Radiation on Image Resolution and Noise,” SPIE Medical Imaging 2006: Physics of Medical Imaging (2006).

R.S. Saunders, E. Samei, and J. Baker, “Effect of Image Quality on Mammographic Accuracy,” Radiology Grand Rounds, Duke University Medical Center, Durham, NC, January 2006. (*Invited Lecture*)

R.S. Saunders, E. Samei, J. Baker, J.Johnson, A. Chawla, and J. Nafziger, “Effect of Image Quality Parameters on the Detection of Mammographic Lesions,” Medical Image Perception Society Conference XI (2005).

R.S. Saunders and E. Samei, “Impact of Digital Displays on the Detection of Breast Lesions,” Era of Hope Conference (2005).

Full-Length Conference Proceeding Articles

R.S. Saunders and E. Samei, “A Monte Carlo Investigation on the Impact of Scattered Radiation on Image Resolution and Noise,” Proc. SPIE **6142** (2006).

Refereed Journal Articles

R.S. Saunders, and E. Samei, “Resolution and Noise Measurements of Selected Commercial Medical Displays,” Med. Phys. **33**, 308-319 (2005).

Conclusions

This year, we have developed a new tool to model scattered radiation in digital radiographic systems. This tool will allow us to better understand how scatter affects image quality as it degrades resolution and noise. Further, we explored the impact of resolution and noise on the detection and discrimination of mammographic lesions. We probed this question using several tools developed last year. We used observer models to analyze a large image set with mammograms emulating those acquired at reduced dose and those displayed on different commercial medical displays. We also conducted an observer experiment with five mammographers who viewed mammograms of several simulated dose levels on three different medical-grade displays. We have begun to analyze this data to assess how resolution and noise affect detection of benign masses, malignant masses, and microcalcifications as well as discrimination of benign and malignant masses. In future work, we will analyze the data from these experiments to understand how resolution and noise separately and jointly affect lesion detection and discrimination.

References

[1] R. S. Saunders and E. Samei,"Characterization of breast masses for simulation purposes," Proc. SPIE **5372**, 242-250 (2004).

[2] R. S. Saunders Jr., E. Samei, and J. A. Baker, "Simulation of Breast Lesions," presented at the 7th International Workshop on Digital Mammography, Durham, NC, 2004.

[3] R. S. Saunders and E. Samei,"A method for modifying the image quality parameters of digital radiographic images," Med Phys **30**, 3006-3017 (2003).

[4] S. Suryanarayanan, A. Karellas, and S. Vedantham,"Physical characteristics of a full-field digital mammography system," Nucl Instrum Methods **533**, 560-570 (2004).

[5] R. S. Saunders and E. Samei,"Resolution and noise measurements of five CRT and LCD medical displays," Med Phys **33**, 308-319 (2006).

Appendices

Appendix I:
R.S. Saunders, and E. Samei, “Resolution and Noise Measurements of Selected Commercial Medical Displays,” Med. Phys. **33**, 308-319 (2005).

Appendix II:
R.S. Saunders and E. Samei, “A Monte Carlo Investigation on the Impact of Scattered Radiation on Image Resolution and Noise,” SPIE Medical Imaging 2006: Physics of Medical Imaging (2006).

Resolution and noise measurements of five CRT and LCD medical displays

Robert S. Saunders, Jr.[a)]
Duke Advanced Imaging Laboratories, Department of Radiology, Duke University Medical Center, Durham, North Carolina 27710, and Department of Physics, Duke University, Durham, North Carolina 27710

Ehsan Samei
Duke Advanced Imaging Laboratories, Department of Radiology, Duke University Medical Center, Durham, North Carolina, 27710, and Departments of Physics and Biomedical Engineering, Duke University, Durham, North Carolina 27710

(Received 9 March 2005; revised 27 October 2005; accepted for publication 14 November 2005; published 13 January 2006)

The performance of soft-copy displays plays a significant role in the overall image quality of a digital radiographic system. In this work, we discuss methods to characterize the resolution and noise of both cathode ray tube (CRT) and liquid crystal display (LCD) devices. We measured the image quality of five different commercial display devices, representing both CRT and LCD technologies, using a high-quality charge-coupled device (CCD) camera. The modulation transfer function (MTF) was calculated using the line technique, correcting for the MTF of the CCD camera and the display pixel size. The normalized noise power spectrum (NPS) was computed from two-dimensional Fourier analysis of uniform images. To separate the effects of pixel structure from interpixel luminance variations, we created structure-free images by eliminating the pixel structures of the display device. The NPS was then computed from these structure-free images to isolate interpixel luminance variations. We found that the MTF of LCDs remained close to the theoretical limit dictated by their inherent pixel size (0.85 ± 0.08 at Nyquist frequency), in contrast to the MTF for the two CRT displays, which dropped to 0.15 ± 0.08 at the Nyquist frequency. However, the NPS of LCDs showed significant peaks due to the subpixel structure, while the NPS of CRT displays exhibited a nearly flat power spectrum. After removing the pixel structure, the structured noise peaks for LCDs were eliminated and the overall noise magnitude was significantly reduced. The average total noise-to-signal ratio for CRT displays was $6.55\% \pm 0.59\%$, of which $6.03\% \pm 0.24\%$ was due to interpixel luminance variations, while LCD displays had total noise to signal ratios of $46.1\% \pm 5.1\%$ of which $1.50\% \pm 0.41\%$ were due to interpixel luminance variations. Depending on the extent of the blurring and prewhitening processes of the human visual system, the magnitude of the display noise (including pixel structure) potentially perceived by the observer was reduced to $0.43\% \pm 0.01\%$ (accounting for blurring only) and $0.40 \pm 0.01\%$ (accounting for blurring and prewhitening) for CRTs, and $1.02\% \pm 0.22\%$ (accounting for blurring only) and $0.36\% \pm 0.08\%$ (accounting for blurring and prewhitening) for LCDs. © *2006 American Association of Physicists in Medicine*. [DOI: 10.1118/1.2150777]

Key words: Image quality, Medical Display, Modulation Transfer Function, Normalized Noise Power Spectrum, Liquid Crystal Display, Cathode Ray Tube

I. INTRODUCTION

For many years, radiographic images were acquired with screen-film systems. A screen-film system bundled detection, image processing, and image display into one device. The advent of digital systems separated these functions into distinct components that could be independently optimized.[1] The image quality of a digital x-ray system, therefore, does not solely depend on the detector, but also on all components of the imaging chain, including the display device utilized.[2] In order to form a complete picture of a system's image quality, one must thoroughly measure the physical characteristics of the display device utilized.

Currently, medical displays rely on two underlying technologies. Based on an older technology, cathode ray tube (CRT) displays use a focused electron beam striking upon a phosphor to create an image.[3] In contrast, liquid crystal display (LCD) devices control the light output from individual pixels with liquid crystals and polarizing filters.[3] The resolution and noise of these display types are governed by different physical processes. The resolution of a CRT display depends on the extent and control of the electron beam. The monitor yields lower resolution at higher luminance levels and at the display peripheries, as the electron beam spreads at these luminance levels and beam projections.[4,5] Furthermore, the resolution of a CRT systematically degrades with age due to deterioration of the electron gun and a necessary increase in electron beam intensity because of a loss of phosphor luminance efficiency.[6,7] In contrast, LCDs allow for very high resolution, often approaching the limit dictated by their pixel size.[8] However, each pixel requires a significant amount of electronics to operate, which leads to considerable structured noise patterns.[9]

TABLE I. Description of the five display systems evaluated in this study. The first five rows are based on manufacturer specifications, while the next two rows reflect quantities measured in our laboratories (Ref. 25). The last row indicates the magnification ratio used for image acquisition, or the number of camera pixels used to image one display pixel.

	Barco MGD 521	Barco MGD 521M	IBM T221	National display systems Nova III	National display systems Nova V
Display Card	Barco MP1H (10-bit)	Barco 5MP2 (10-bit)	NVIDIA Quadro FX 4000 (32-bit floating point)	RealVision MD3mp (10-bit)	RealVision MD5mp (10-bit)
Type	CRT	CRT	LCD	LCD	LCD
Additional properties	p45 phosphor	p45 phosphor	Color display		
Pixel pitch (mm)	0.148	0.148	0.125	0.207	0.165
Matrix size	2048×2560	2048×2560	3840×2400	1536×2048	2048×2560
Active display area	304 mm $\times$ 380 mm	304 mm $\times$ 380 mm	478 mm $\times$ 299 mm	318 mm $\times$ 424 mm	338 mm $\times$ 422 mm
L_{min}(Cd/m^2)	0.52	0.60	0.83	0.43	0.52
L_{max}(Cd/m^2)	308	316	235	369	371
Magnification ratio for measurement	29.6	29.6	25.0	41.4	33.0

Several researchers have considered display resolution when evaluating image quality for soft-copy displays.[7,10,11] The resolution of a display does influence the information content of an image, but other factors also affect the displayed image. For instance, investigators have more recently given attention to the noise properties of display devices.[9,12] As the magnitude and spatial frequency content of noise may impact the overall clinical utility of a display device, one must quantify both the resolution and noise of these displays to form an accurate picture of display performance.

The purpose of this work is to measure the resolution and noise properties of several medical displays, including both CRT and LCD technologies. Two key metrics were examined, the modulation transfer function (MTF) and normalized noise power spectrum (NPS), which summarize the resolution and noise properties of the display, respectively.[13–16] In addition, this paper introduces new methods for isolating the structured noise of CRTs and LCDs.

II. METHODS AND MATERIALS

A. Display description

Five different medical-grade display devices were evaluated, as listed in Table I, representing both cathode ray tube (CRT) and liquid crystal display (LCD) devices. All displays were calibrated to the Digital Imaging and Communications in Medicine (DICOM) standard according to the display manufacturer before measurements. All experiments were conducted in a room with controlled low ambient lighting set to 9 lux illuminance.

B. Camera description and evaluation

The physical characteristics of the display devices were measured using a charge-coupled device (CCD) camera (XCD-SX900, Sony Corporation, Tokyo, Japan) equipped with a macro lens (Rodgen 1:4, 28mm, Rodenstock, Munich, Germany). The camera captured images of 1280×960 pixels in size with a CCD chip of 6.5×4.8 mm employing a pixel size of 4.65×4.65 μm. The lens was set to its highest magnification, such that one camera pixel imaged a 0.0050 mm $\times$ 0.0050 mm area in the focal plane. The lens used a small aperture with a f-stop of f/11 to ensure the camera had a relatively large depth of field, which allowed objects near the true focal plane to also be captured with relative sharpness. The camera was secured on a custom gantry, offering coarse linear movement as well as fine linear movement with 0.01 mm precision (See Fig. 1). Data were transferred to a PC workstation through a FireWire connection using an image acquisition software (ImageJ; Research Services Branch, National Institute of Mental Health, Bethesda, Maryland).

To correct for any gain nonuniformities from the camera, the flat-field response of the camera was measured. As the

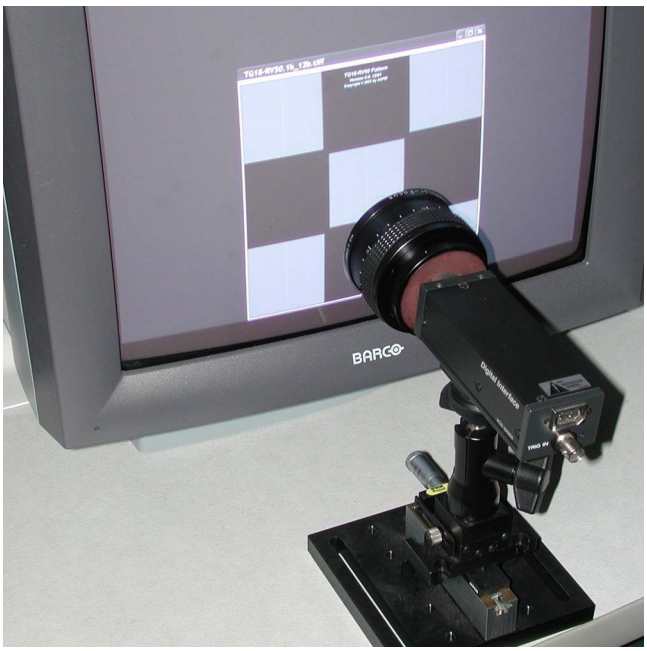

FIG. 1. High-quality CCD camera mounted on custom gantry for measurement of display characteristics. The gantry was capable of both coarse and fine linear movement.

gain characteristics of the camera depended on luminance, this measurement was conducted for each of the luminance levels used during display measurements. The light source consisted of a standard radiographic lightbox (X-ray Film Illuminator, S&S X-ray Products, Brooklyn, NY) covered with a neutral density filter to achieve a given luminance. Opal diffusing glass (Edmund Optics, Barrington, NJ) was placed next to the filter, which created a near Lambertian source. The camera was supplemented with a cone constructed of graphics arts black paper with velvet-type, black, light absorbing cloth. This ensured that the camera only captured light that had come through the diffuser. Finally, the diffuser was positioned several centimeters behind the camera focus; otherwise this may have revealed small nonuniformities in the diffuser, affecting the results. The camera acquired ten images at each luminance level. A gain map was formed from the average of these images. All subsequent display measurements were corrected by the appropriate gain map (corresponding to the approximate average luminance of the display) as

$$I'(x,y) = \frac{\bar{g}(L) - \beta}{G(L;x,y) - \beta}[I(x,y) - \beta], \quad (1)$$

where $G(L;x,y)$ represents the average flat-field image at luminance L with mean $\bar{g}(L)$, $I(x,y)$ refers to the uncorrected image, β represents the pixel value at zero luminance value, and $I'(x,y)$ corresponds to the corrected image.

The inherent resolution performance of the camera was computed using the edge technique. The camera acquired an image of an edge of a 1 mm square on a glass slide resolution target (1951 USAF slide, Edmund Industrial Optics, Barrington, NJ). The slide was backlit using the same lightbox covered with a neutral density filter to achieve a luminance level of 269 cd/m^2. The MTF was calculated from the edge image using a previously published method.[17] First, a Radon transformation was applied to the data to determine the line angle with 0.01 deg accuracy. The image data were then projected along lines parallel to the edge transition, forming the edge spread function (ESF). This projection was applied in a 1.19 mm $\times$ 1.19 mm region centered on the edge and the data were placed into bins of 0.1 pixel in size. A fourth-order moving polynomial fit provided modest smoothing for the ESF while minimizing noise. The ESF was subsequently differentiated using a discrete derivative to form the line spread function (LSF). The tails of the LSF were forced to zero using a Hann window of 0.5 mm. Finally, the MTF was computed from the normalized fast Fourier transform (FFT) of the LSF.

C. Measurement of display resolution

The display resolution was measured using the line spread function (LSF) technique. The TG18-RV50 and TG18-RH50 test patterns provided vertical and horizontal line patterns, respectively.[7,18] These patterns utilized subtle lines, with 12% pixel value contrast from the background, in order to satisfy the quasilinear system requirements of the MTF measurements. The CCD camera acquired magnified images of the displayed line pattern for each display device, where the line appeared approximately in the center of its field of view.

One caveat to the MTF measurement process concerns the concept of focus. While the camera must be in focus to capture correct information, the literature devotes few references to quantitative definitions of focus. As out of focus images are relatively blurred compared to their in-focus counterparts, the level of detail in a focused image is maximized, thus maximizing the standard deviation of the image.[11] As the camera in this study used a small aperture, it offered a relatively large depth of field. This allowed the camera to provide in focus images of LCDs that are composed of several thin, closely spaced planes of electronics and optical equipment. Experimentally, focusing was achieved by placing the camera where the image visually appeared to be in focus. The camera was then moved around that initial position sequentially until the standard deviation of the image was maximized. The image that possessed the highest standard deviation was considered to be in focus.

Our MTF measurement technique aimed to characterize the MTF of displays independent of noise properties for the display. As CRT displays and LCDs possessed different types of structured noise, the structured noise was removed from the line images using two different methods. For CRT displays, a structure map was created of the raster lines by averaging the image data along the raster line direction. The raster map was then subtracted from the line image to create a structure-free image. This procedure only averaged over areas of the image not containing the line test pattern. For vertical line patterns where the line pattern was perpendicular to the raster structure, this method could create a map of all raster lines. However, for horizontal line patterns, the line pattern was parallel to the raster lines and thus the area immediately surrounding the line pattern was excluded from this correction procedure. For LCDs, we averaged 20 pictures of the line pattern and 20 pictures of the pixel background. The average background image was then subtracted from the average line image.[11] The MTF was computed from these structure-free line images.

The MTF was calculated from the acquired line images using a modified version of the MTF calculation routine described in Sec. II B. To calculate the line angle, the image was blurred with a Gaussian kernel and then thresholded. The magnitudes for the Gaussian blur and the thresholds were determined from statistical analysis of the experimentally acquired images to give the best estimate of the line angle unaffected by noise. The angle of this thresholded line was then determined through a linear regression. Next, the pixel values of the original image were binned along lines parallel to the line pattern to form the line-spread function. This binning occurred in a 2.5 mm $\times$ 2.5 mm region centered on the line pattern with bins of one camera pixel in size. To correct for background trends in the data, a line was fit to the tails of the LSF.

Signal processing of the LSF preserved the central line area, defined as four display pixels on either side of the line peak, while processing the data in the tails of the LSF. A modified Hann window of one display pixel in width was

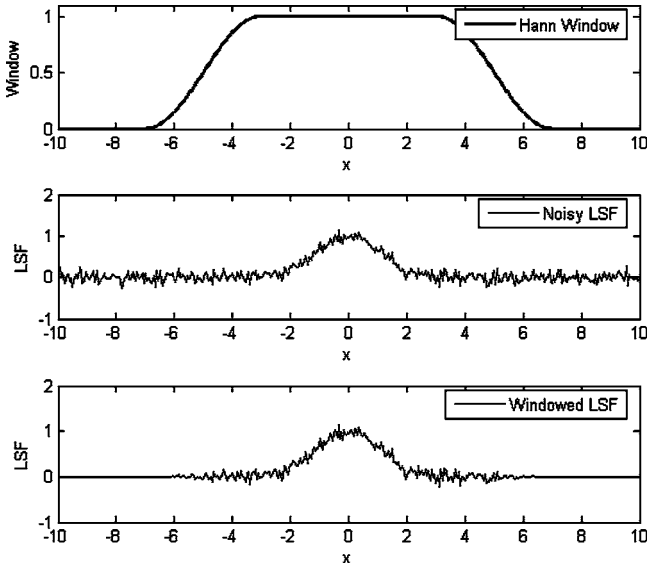

FIG. 2. Schematic of windowing procedure for the line spread function. The top curve shows a simple example of the Hann window. The middle subfigure illustrates an example noisy line spread function. The final subfigure shows the line spread function after application of the Hann window. This forces the edges of the LSF to zero to meet the criteria for Fourier analysis.

utilized to force the tails of LSF to zero, while protecting the central line area. The window took the following functional form

$$H(x)=\begin{cases} 1 & |x|<a \\ \left(\frac{1}{2}\right)\left(1+\cos\left[\pi\frac{|x|-a}{b-a}\right]\right) & a<|x|<b \\ 0 & |x|>b \end{cases}, \qquad (2)$$

where x represents the distance from the central peak of the line spread function, a denotes the length of the protected central line area (i.e., four display pixels in our routine) and $b-a$ corresponds to the distance over which the Hann window goes to zero (i.e., one display pixel in this routine). Figure 2 illustrates a simple case of applying the window function to a noisy line spread function.

Finally, the MTF was computed as the normalized FFT of the LSF. To account for the camera MTF and display pixel size, the results were divided by the MTF of the CCD camera and the sinc function corresponding to the display pixel size as

$$MTF_{\text{display}}(u)=\frac{MTF_{\text{measured}}(u)}{MTF_{\text{camera}}(u)\text{Sinc}(u\delta)}, \qquad (3)$$

where $\text{MTF}_{\text{camera}}$ represents the camera MTF, $\text{MTF}_{\text{measured}}$ refers to the experimentally measured MTF, δ describes the pixel size, and $\text{MTF}_{\text{display}}$ corresponds to the true MTF of the display device.

D. Measurement of display noise

The noise was evaluated using Fourier analysis of uniform images. For each display device, the camera acquired magnified images of a uniform gray area of the TG18-NS50 test pattern.[18] Similar to the resolution measurements, several preliminary images were acquired to determine whether the images were in focus. The frequency content of the image noise was evaluated in terms of the normalized noise power spectrum (NPS).[17,19] First, a region (3.8 mm $\times$ 5.1 mm) was extracted from the center of the image. This method assumed that the pixel structure in this region would be representative of the other areas of the display. This assumption should be satisfied by most displays constructed using modern manufacturing methods, producing similar pixel structures across the display. The region was then segmented into 117 overlapping regions of interest (ROIs) of 256×256 pixels(1.3 mm $\times$ 1.3 mm). The ROIs overlapped with each of their nearest neighbors by 50%. Each region was scaled by its mean pixel value to form the relative signal. A Hamming window was applied to each ROI to ensure the ROI approached zero at its edges. After computing the two-dimensional FFT of each ROI, the NPS was computed as the average of the absolute magnitude squared of each FFT.

In order to further understand the noise properties of the displays, the total noise was decomposed into two different categories following an analysis similar to a previous study.[9] This separated the total noise into two classes corresponding to different physical properties of the display: interpixel and intrapixel variations. The first category, interpixel variations, included the differences in luminance between pixels. CRT phosphor structured noise could be considered as interpixel noise, while for a LCD, such fluctuations were often caused by the nonuniform thickness of the liquid crystal elements across the display. The physical structure of the pixel caused the second form of variation, intrapixel noise. Whereas an observer would experience both forms of noise when viewing images on a display, this analysis explored how much of the total noise of a display was due to interpixel luminance variations and the pixel structure (i.e., intrapixel) components.

To isolate the interpixel luminance variations, the images were processed to remove the physical structure of the pixels or intrapixel variations. For CRT displays, the pixel structure was removed by the raster profile subtraction method (see Sec. II C). For LCDs, the following procedure was followed. The experimentally acquired uniform images were rotated to align their pixels along the horizontal direction. Due to careful camera positioning, this rotation angle remained below 1°. The rotated image was summed across both the horizontal and vertical directions. These horizontal and vertical traces showed a peak at the center of each subpixel, such that a full pixel could be constructed by counting the appropriate number of horizontal and vertical peaks. The procedure then created a pixel grid across the image, as displayed in Fig. 3(a). The routine looped through the grid and centered each grid rectangle on the pixel center. This pixel grid was visually inspected to ensure that the grid properly enclosed the pixels. An image of interpixel luminance variations was then formed where each grid rectangle was replaced by its mean luminance value. While this process removes the subpixel

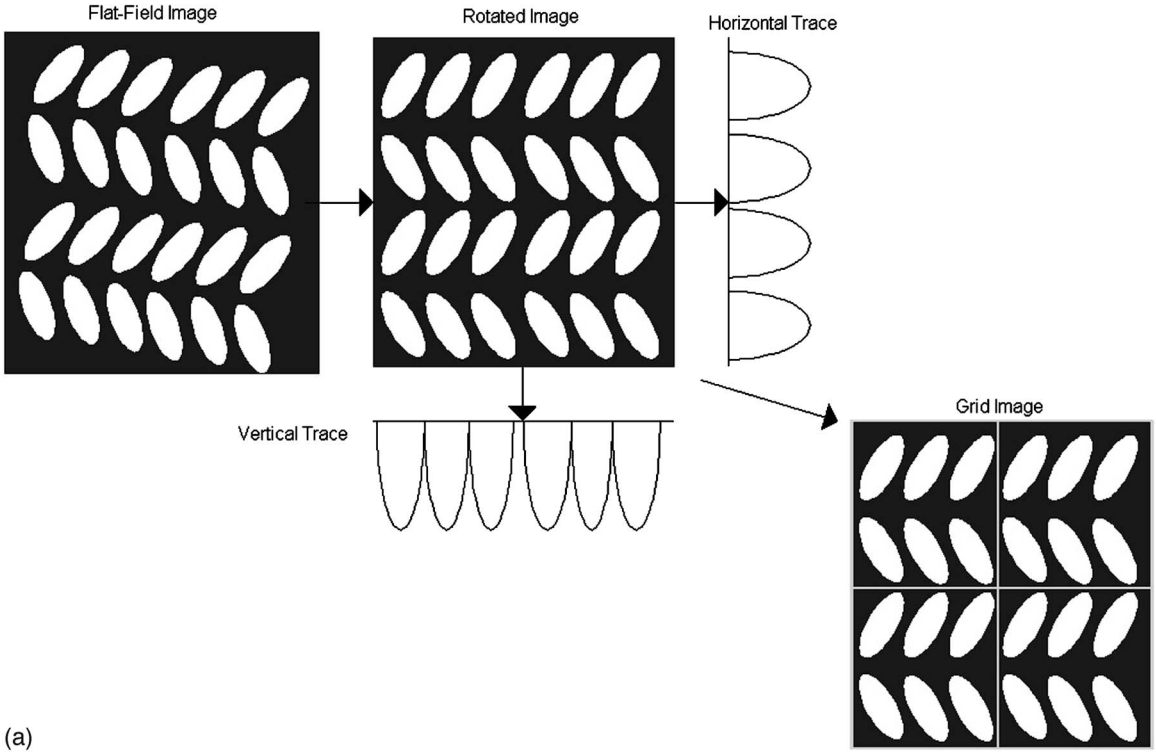

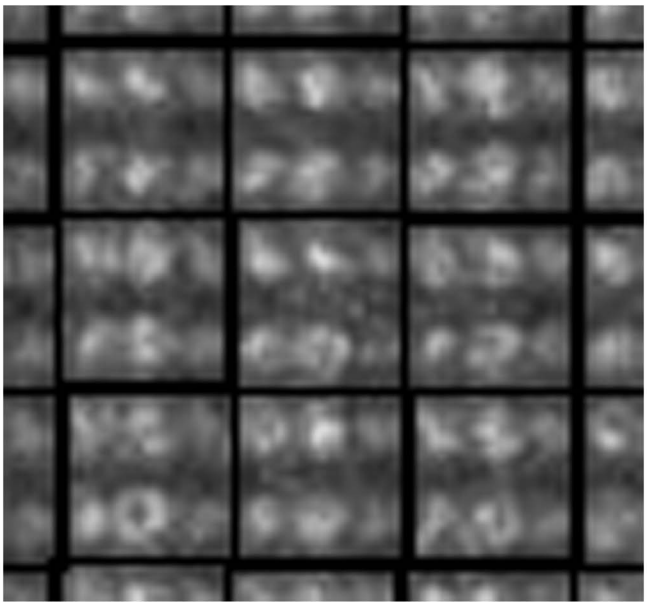

FIG. 3. Graphical description of pixel alignment procedure (a) and example of pixel alignment procedure on region of IBM T221 display (b). The dark lines indicate the borders of the pixel box.

structures for the LCD, the inherent pixelation effects associated with digital images remains. An example of this pixel alignment procedure is shown in Fig. 3(b). The NPS was recalculated from the pixel-structure-removed LCD and CRT images to examine the contribution of pixel structure to the total display noise.

III. RESULTS

Figure 4 illustrates the inherent MTF and NPS of the CCD camera. The camera provided a very high MTF over the frequency range of interest, declining only to 0.88 at 10 mm^{-1}. The MTFs of all displays were corrected by the MTF of the camera to present an accurate estimate of display resolution. However, the noise images were not corrected by the MTF, as this would unacceptably amplify the high-frequency noise.[10] The camera NPS corresponded to white noise with a very low magnitude of $5 \cdot 10^{-9}$ to 10^{-8} mm^2 over the entire frequency range of interest. This indicates that the camera added minimal noise to the acquired images.

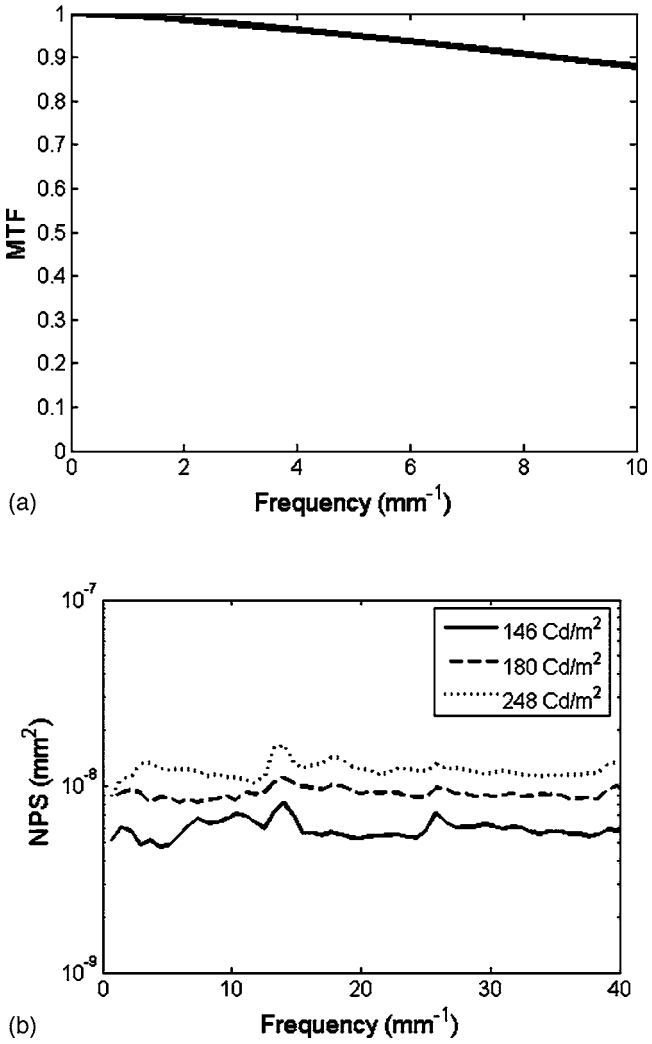

FIG. 4. Plot of the (a) MTF and (b) radial trace of the NPS of the CCD camera. The MTF remains high over the frequency range of interest. The NPS magnitude remains white and low over the entire frequency range of interest.

Figure 5 shows the measured MTF for the five display devices over the frequency range of interest from zero frequency to the Nyquist frequency dictated by the display pixel size. The first two graphs [Figs. 5(a) and 5(b)] pertain to CRT display devices while the final three plots [Figs. 5(c)–5(e)] pertain to LCDs. The LCD MTFs stayed close to unity throughout the clinically relevant frequency range of 0–4 mm^{-1}, while the MTFs for CRT displays contained far less power at higher frequencies. Each plot includes the MTF calculated along the horizontal and vertical directions in order to indicate any potential asymmetries in resolution. The horizontal and vertical MTFs remained similar for the LCDs, which indicated little asymmetry in the resolution properties of these display devices. This contrasted with the CRT displays, which exhibited notable differences between the horizontal and vertical directions, as different physical properties control the resolution in each direction.[6] As noted in Sec. II C, the horizontal MTF included some effects from the raster line pattern, which contributed some noise to the measured MTF.

Figure 6 illustrates traces of the normalized noise power spectrum of the total system noise for five display devices. The NPS for the CRT displays showed one peak in the vertical direction corresponding to the raster line structure. In contrast, the NPS for the LCDs revealed multiple peaks from the subpixel structure. In addition, the overall noise magnitude for the CRT displays was lower than that of the LCDs. Figure 7 shows, for example, two-dimensional NPS presented in a logarithmic scale for an example CRT and an example LCD. The CRT NPS exhibited only two peaks along the vertical axis while the LCD NPS presented a complex structure across the frequency range.

Figure 8 illustrates the NPS calculated from the images after pixel structure removal. The NPS for CRTs no longer exhibited a peak in the vertical direction, as the raster structure was eliminated, while the magnitude remained largely constant. For LCDs, the overall noise magnitude dropped significantly. In addition, the shape of the NPS changed, such that the shape now resembled the sinc function corresponding to the display pixel size. Figure 9 shows two examples of two-dimensional NPS after the structure removal procedure. Compared to their counterparts in Fig. 7, these NPS of the interpixel luminance variations exhibited few peaks from the pixel structure, but peaks due to the inherent pixelation effects remained. Table II summarizes the magnitude of the noise for displays before and after the structure removal process. As expected, the pixel structure removal procedure greatly lowered the overall variance for LCDs, indicating that subpixel structure acts as the primary source of noise for LCDs. In contrast, the variance for CRT displays stayed similar to the noise variance without pixel structure removed, suggesting that interpixel luminance variations compose the primary form of noise for this display type.

IV. DISCUSSION

To fully quantify the performance of a digital x-ray imaging system, the properties of the display device must be considered. This work measured both the resolution and noise of two medical display technologies using a robust methodology for the in-field measurement of display resolution in clinical settings. The measurement procedure corrected for differing pixel structure, which isolated the structured noise from luminance variations between pixels. If implemented commercially, this methodology may be used by institutions interested in display characterization.

Our MTF calculation procedure was very similar to previous work by Samei and Flynn[7] with two notable differences. First, the line angle was computed using a linear regression of the thresholded line, as opposed to a Hough transform. The regression showed less sensitivity to the structured noise common to LCDs. Second, in order to reduce the impact of display noise on our MTF results,

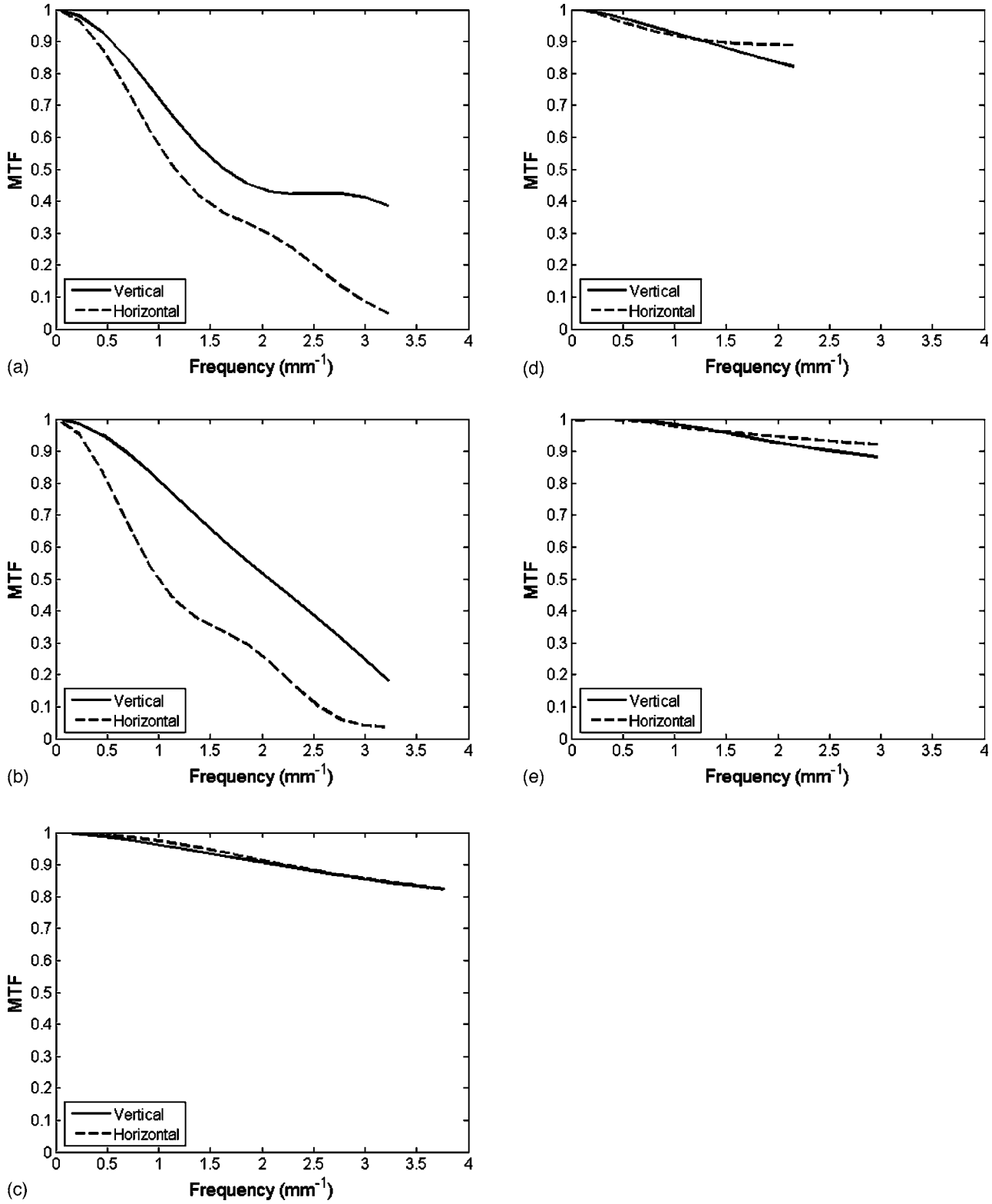

FIG. 5. Measured MTFs for (a) Barco MGD 521, (b) Barco MGD 521M, (c) IBM T221, (d) NDS Nova III, and (e) NDS Nova V displays. For the CRT displays, the horizontal and vertical MTFs diverge due to the difference in the processes impacting resolution in the two directions. For the LCDs, little asymmetry exists between the horizontal and vertical axes and the MTF remains high over the frequency range of interest.

we removed the pixel structure noise from the line pattern images. For LCDs, the structure removal was similar to that of Roehrig *et al.*[11] However, this methodology proved difficult to implement for CRT displays because of temporal luminance variations. This led to the use of the raster line correction procedure, which operated on a single image.

Our noise computation procedure differed from previous measurement algorithms in the following ways. Unlike

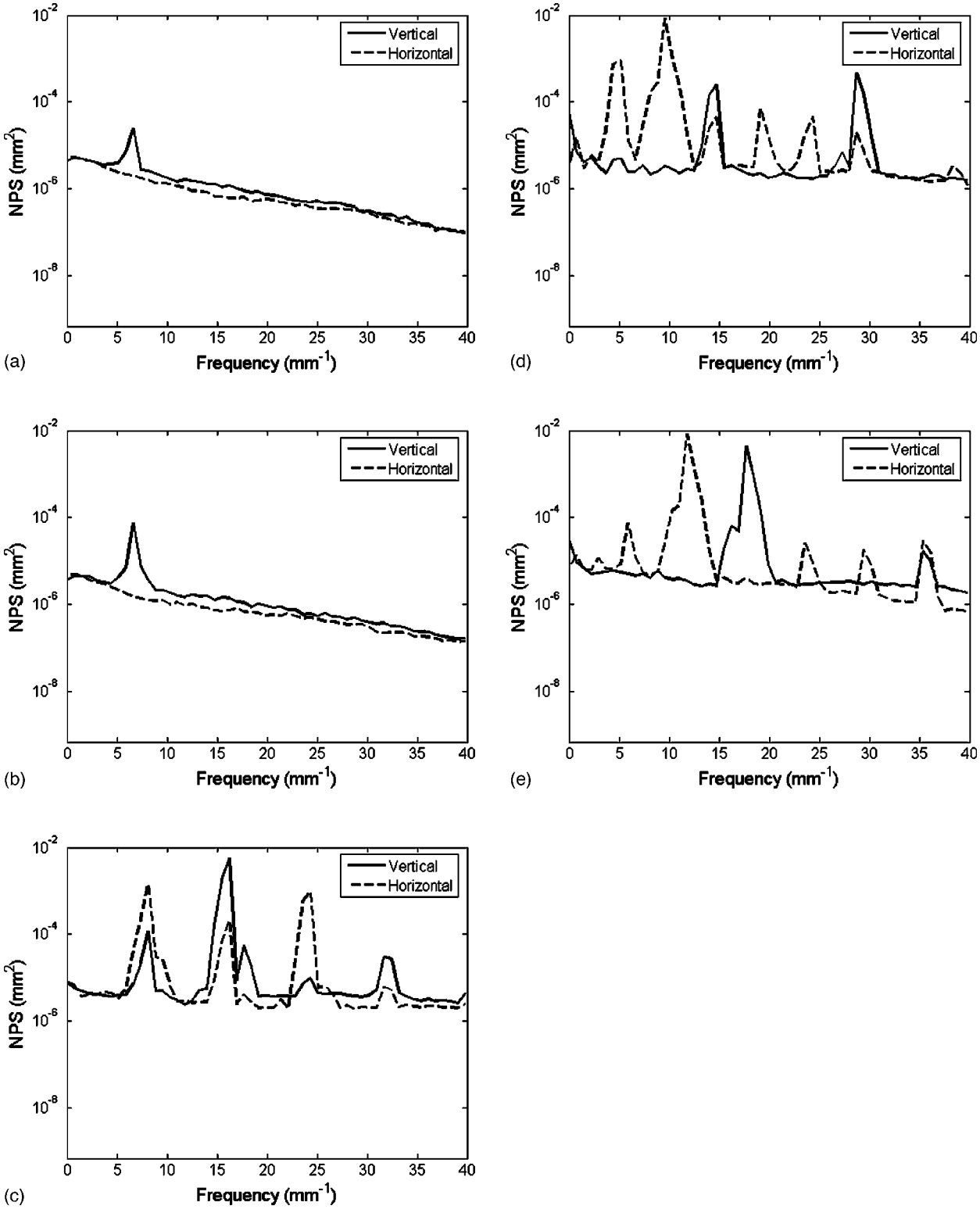

FIG. 6. Horizontal and vertical traces of the NPS of the total system noise for (a) Barco MGD 521, (b) Barco MGD 521M, (c) IBM T221, (d) NDS Nova III, and (e) NDS Nova V displays. The pixel structure causes notable peaks in the NPS for the LCD displays, while the raster structure of the CRT displays led to one peak in the vertical direction.

Muka *et al.*[20] we did not correct the uniform images by the MTF of the measurement camera, as this led to an undesirable amplification of high-frequency noise. However, we acquired all images with a narrow aperture, using only the central area of the lens and a high magnification. These two steps led to minimal resolution degradation and distortion by the lens. Similar to Badano *et al.*[9] we separated the interpixel and intrapixel noise contributions. However, we did not use

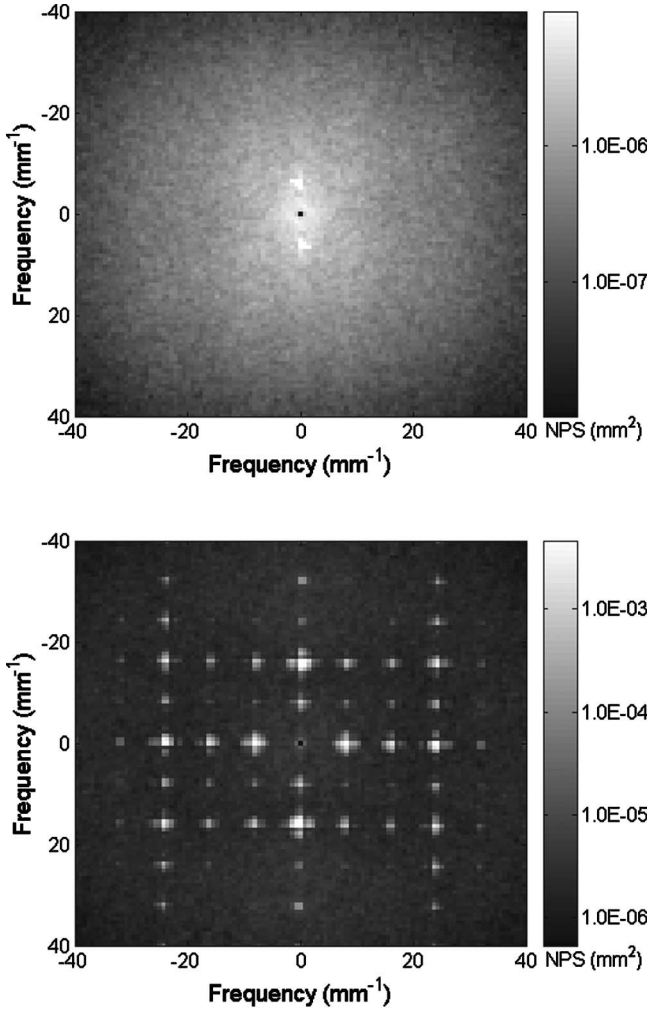

FIG. 7. Two-dimensional NPS displayed in a logarithmic scale for (a) Barco MGD 521 and (b) IBM T221 displays. The raster line leads to vertical peaks for the CRT display, while the pixel structure of the LCD produces multiple peaks across the NPS.

their pixel registration methodology to remove LCD pixel structure because of its computational cost. Instead, we examined other pixel features for LCDs to develop a pixel grid. Similar to that study, however, our pixel correction algorithm noticeably lowered the overall image noise due to the elimination of the pixel structure.

Before any measurements took place, considerable effort was devoted to characterize the properties of the CCD camera. This study included corrections for the experimentally measured MTFs by the inherent MTF of the CCD camera. At 4 mm^{-1}, the magnitude of this correction was 3.7%. In addition, careful gain calibration was performed to minimize any distortion by the lens. The magnitude of gain calibration was as high as 7.2%, with an average of 1.1%. Taken together, these two effects may have an appreciable effect on the measured MTF and NPS of a display device.

This research used a high-optical magnification to capture high-quality images of the display device. This allowed us to characterize the pixel structure with high precision, as the images showed the fine detail of the subpixel elements. In addition, this minimized the contribution of camera blur. However, using a high-optical magnification reduced the camera field of view. Therefore, our analysis had less power in characterizing low-frequency variations often recognized as nonuniformities. This paralleled the work of previous investigators in not characterizing broad nonuniformities as noise.[9]

The NPS results showed that luminance differences between pixels constituted the primary noise source for CRT displays. The pixel structure removal eliminated the peak in the NPS, corresponding to the frequency of the raster lines, but did not alter the magnitude of the NPS. In contrast, pixel structure served as the primary noise source for LCDs. After removing structured noise, the shape of the NPS changed and the overall magnitude of the NPS dropped dramatically. This indicated that pixel structure remains the dominant source of noise for LCDs, confirming the results of Badano *et al.*[9] However, the pixel corrected NPS curves of CRT and LCD devices should be compared with caution as the pixel structure removal methodology differed for the two display types, due to differing pixel structures. This analysis explored what factor, interpixel luminance variations or pixel structure (intrapixel variations), represented the primary source of noise for each display type.

To understand the magnitude of the noise levels in Table II, these metrics can be compared to the quantum noise level in clinical images. For instance, the noise levels in representative mammograms and chest radiographs, including quantum noise and electronic noise, is approximately 1%–3% in terms of the standard deviation to the mean image grayscale value. The display noise values, as summarized in Table II, are comparable to these figures. This illustrates the importance and potential impact of display noise on diagnostic performance.

The noise-to-signal ratios calculated in Table II contain all noise in the image. However, two processes could reduce the impact of noise on human perception. First, there have been indications that human observers can prewhiten structured patterns from images, thus reducing their potential impact.[21] In the case of total prewhitening, the right columns of Table II would be more representative of display noise than the left columns. However, it is uncertain to what extent humans can prewhiten the structured noise of display devices. Second, human observers do not perceive the different spatial frequencies of a scene with equal acuity. One can estimate how much of the display noise could be perceived by a human observer by filtering the measured NPS results with the human visual response function $V(\rho)$ (Ref. 22) as

$$\mathrm{NPS}_{\mathrm{filtered}}(u,v) = \mathrm{NPS}_{\mathrm{measured}}(u,v)\left|V(\rho)\right|^2,$$

$$V(\rho) = \left|\eta\rho^{a_1}\cdot e^{-a_2\rho^{a_3}}\right|^2 \tag{4}$$

where ρ describes the radial spatial frequencies of the image in cycles/millimeters assuming a viewing distance of 40 cm, η normalizes $V(\rho)$ to one as its maximum value, and parameters (a_1, a_2, a_3) equal (1.5, 3.22, 0.68). The areas under the filtered NPS can be used as a measure of perceived noise.

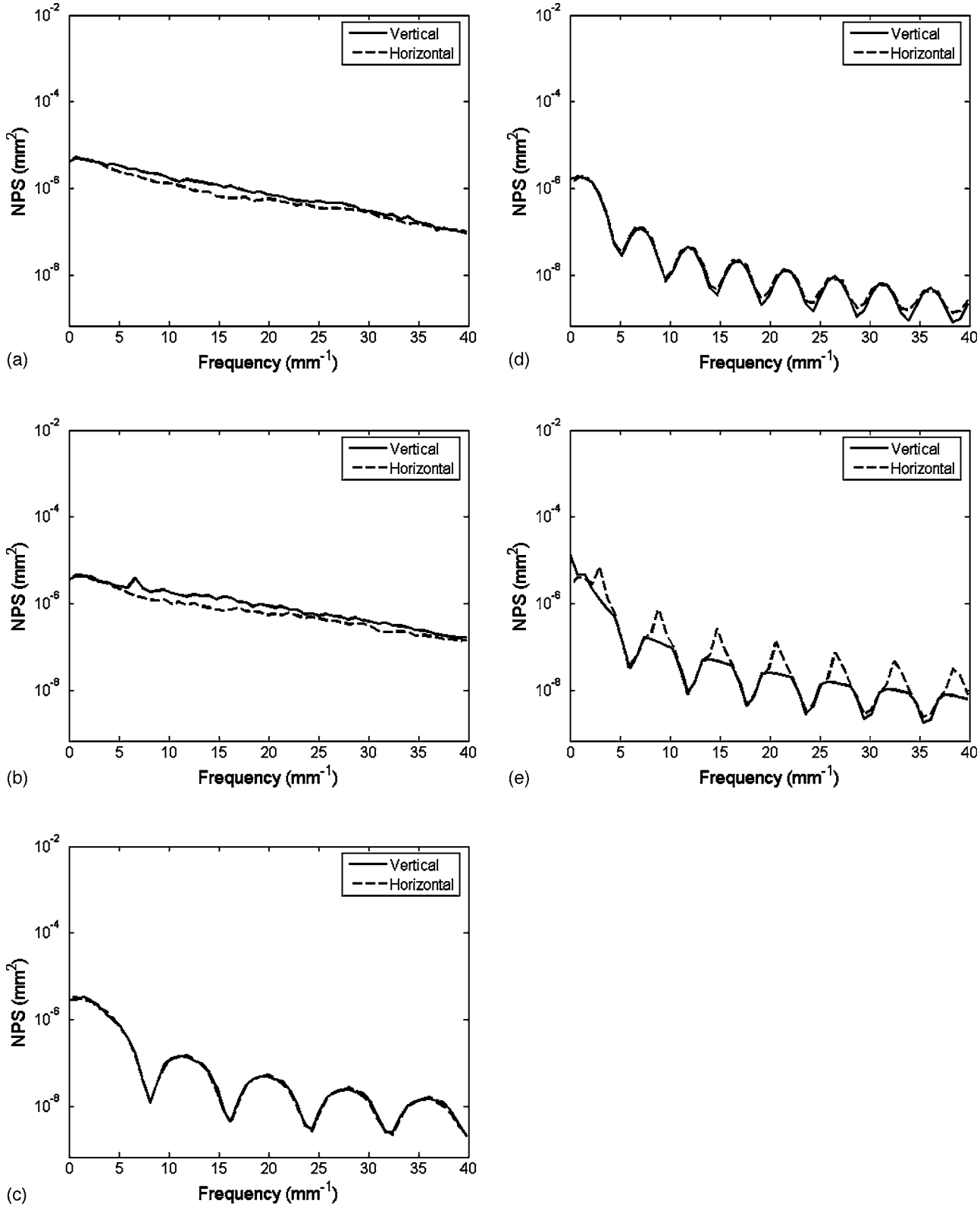

FIG. 8. After correcting for pixel structure, the noise variance drops dramatically. This may be seen in the horizontal and vertical traces of the NPS for (a) Barco MGD 521, (b) Barco MGD 521M, (c) IBM T221, (d) NDS Nova III, and (e) NDS Nova V displays.

The results, shown in Table III, indicate that the majority of pixel structured noise of LCDs will be blurred by the human visual system. The blurring was more effective for the nine megapixel LCD tested given its smaller pixel structure.

Considering the extent of possible prewhitening and frequency filtering processes, the above analysis only serves as a preliminary step in understanding the visual relevance of display noise. As the quantum noise figures noted previously

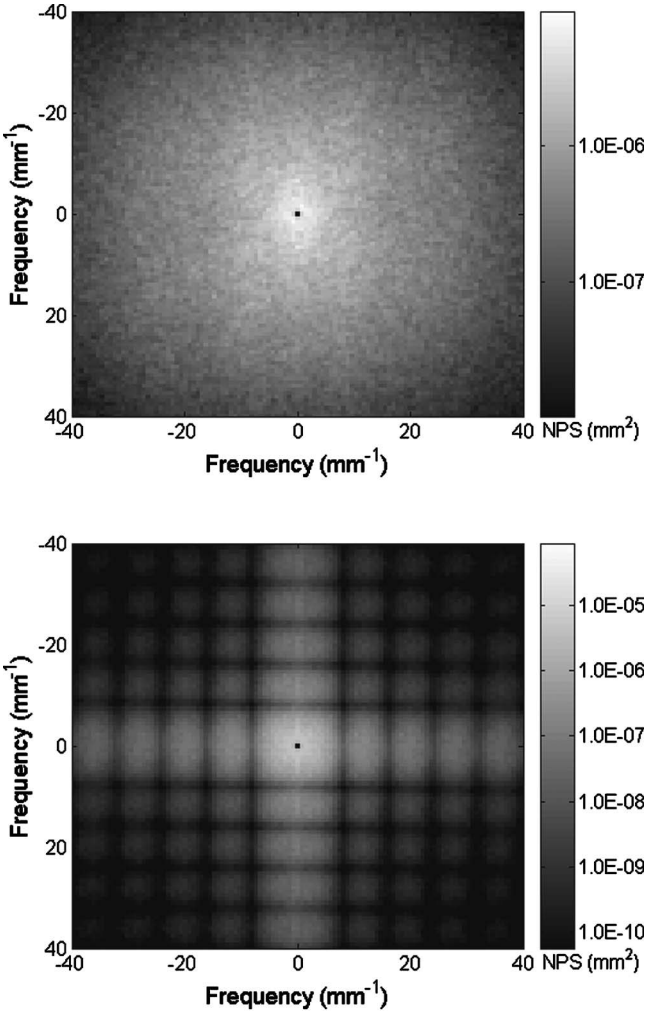

FIG. 9. Two-dimensional NPS calculated from the interpixel luminance noise displayed in a logarithmic scale for (a) Barco MGD 521 and (b) IBM T221 displays. The structure removal procedure eliminates many of the NPS peaks. While this removed the subpixel structure for the LCD display, the inherent pixelation effects remain, as evidenced by the low amplitude regular peaks.

do not compensate for the human visual response, these new noise-to-signal ratios for displays cannot be directly compared to detector noise levels. In addition, these noise figures are not reduced to detectability indices for specific clinical tasks.[23,24] Nonetheless, physical measurements, as undertaken in this study, form a necessary first step in characterizing a display system. Our future work will include observer experiments in order to more fully understand how the resolution and noise characteristics of displays affect clinical performance.[9,24]

TABLE II. Noise-to-signal ratio (standard deviation divided by the mean) for the CRT and LCD displays before and after the pixel structure removal procedure. These numbers were computed from the two-dimensional NPS using Parseval's theorem.

Manufacturer and model	Noise-to-Signal Ratio ($\sigma/\langle x\rangle$) Without pixel structure removal (%)	With pixel structure removal (%)
Barco MGD 521	6.13	5.86
Barco MGD 521M	6.97	6.20
IBM T221	42.45	1.67
NDS Nova III	43.81	1.03
NDS Nova V	51.88	1.80

TABLE III. Perceivable noise-to-signal ratio. After compensating for the transfer properties of the human eye, the noise-to-signal ratios decrease dramatically. This suggests that the human observer may not perceive much of the structured noise from the display devices. These numbers were computed from the two-dimensional NPS filtered by the human visual response and using Parseval's theorem.

Manufacturer and model	Noise-to-Signal Ratio ($\sigma/\langle x\rangle$) Without pixel structure removal (%)	With pixel structure removal (%)
Barco MGD 521	0.44	0.41
Barco MGD 521M	0.42	0.39
IBM T221	0.78	0.36
NDS Nova III	1.20	0.29
NDS Nova V	1.08	0.44

V. CONCLUSIONS

This paper reports an assessment of image quality for five different commercial display devices representing both CRT and LCD technologies. The findings confirm that LCDs offer higher MTFs than CRT displays. Yet, the resolution advantages of LCDs must be considered in light of their noise properties. The CRT displays show a lower MTF, but also demonstrate lower noise. Finally, this study introduces a new means of isolating interpixel variations for both CRT and LCD devices, which will facilitate the noise comparison between monitors using different pixel structures.

ACKNOWLEDGMENTS

The authors wish to thank Annahita Farschi for her assistance in display measurements. The authors also thank Frank Gerber, formerly of National Display Systems, and Mark Hanson and Ken Compton of National Display Systems for lending the NDS displays, and BarcoView, LLC for its support in display calibration. The authors also thank Hans Roehrig for several helpful discussions on camera focusing techniques. This work was supported in part by federal Grant No. NIH R21-CA95308 and USAMRMC W81XWH-04-1-0323.

[a]Electronic mail: Saunders@phy.duke.edu

[1]R. S. Saunders, J., E. Samei, J. L. Jesneck, and J. Y. Lo, "Physical characterization of a prototype selenium-based full field digital mammography detector," Med. Phys. **32**, 588–599 (2005).
[2]J. Fan, W. J. Dallas, H. Roehrig, and E. A. Krupinski, "Improving visualization of digital mammograms on the CRT display system," Proc. SPIE **5029**, 746–753 (2003).
[3]H. Roehrig, J. Fan, A. Chawla, and K. Gandhi, "The liquid crystal display (LCD) for medical imaging in comparison with the cathode ray tube display (CRT)," Proc. SPIE **4786**, 114–131 (2002).
[4]T. Mertelmeier "Why and how is soft copy reading possible in clinical practice?," J. Digit Imaging **12**, 3–11 (1999).
[5]E. Muka, H. R. Blume, and S. J. Daly, "Display of medical images on CRT soft-copy displays: A tutorial," Proc. SPIE **2431**, 341–359 (1995).

[6]K. D. Compton, "Factors affecting CRT display performance: Specifying what works," Proc. SPIE **3976**, 412–423 (2000).
[7]E. Samei and M. J. Flynn, "A method for in-field evaluation of the modulation transfer function of electronic display devices," Proc. SPIE **4319**, 599–607 (2001).
[8]H. R. Blume, P. M. Steven, M. E. Cobb, A. M. K. Ho, F. Stevens, S. Muller, H. Roehrig, and J. Fan, "Characterization of high-resolution liquid crystal displays for medical images," Proc. SPIE **4681**, 271–292 (2002).
[9]A. Badano, R. M. Gagne, R. J. Jennings, S. E. Drilling, B. R. Imhoff, and E. Muka, "Noise in flat-panel displays with subpixel structure," Med. Phys. **31**, 715–723 (2004).
[10]A. Badano, S. J. Hipper, and R. J. Jennings, "Luminance effects on display resolution and noise," Proc. SPIE **4681**, 305–313 (2002).
[11]H. Roehrig, J. Gaskill, J. Fan, A. Poolla, and C. Martin, "In-field evaluation of the modulation transfer function of electronic display devices," Proc. SPIE **5367**, 456–463 (2004).
[12]J. Fan, W. J. Dallas, H. Roehrig, E. A. Krupinski, K. Gandhi, and M. K. Sundareshan, "Spatial noise of high-resolution liquid-crystal displays for medical imaging: Quantitative analysis, estimation, and compensation," Proc. SPIE **5367**, 433–443 (2004).
[13]H. Fujita, K. Doi, and M. L. Giger, "Investigation of basic imaging properties in digital radiography.6. Mtfs of II-TV digital imaging-systems," Med. Phys. **12**, 713–720 (1985).
[14]C. D. Bradford, W. W. Peppler, and J. M. Waidelich, "Use of a slit camera for MTF measurements," Med. Phys. **26**, 2286–2294 (1999).
[15]M. B. Williams, P. A. Mangiafico, and P. U. Simoni, "Noise power spectra of images from digital mammography detectors," Med. Phys. **26**, 1279–1293 (1999).
[16]A. Workman and D. S. Brettle, "Physical performance measures of radiographic imaging systems," Dentomaxillofac Radiol., **26**, 139–146 (1997).
[17]R. S. Saunders and E. Samei, "A method for modifying the image quality parameters of digital radiographic images," Med. Phys. **30**, 3006–3017 (2003).
[18]E. Samei, A. Badano, D. Chakraborty, K. Compton, C. Cornelius, K. Corrigan, M. J. Flynn, B. Hemminger, N. Hangiandreou, J. Johnson, D. M. Moxley-Stevens, W. Pavlicek, H. Roehrig, L. Rutz, J. Shepard, R. A. Uzenoff, J. Wang, and C. E. Willis, "Assessment of display performance for medical imaging systems: Executive summary of AAPM TG18 report," Med. Phys. **32**, 1205–1225 (2005).
[19]M. J. Flynn and E. Samei, "Experimental comparison of noise and resolution for 2k and 4k storage phosphor radiography systems," Med. Phys. **26**, 1612–1623 (1999).
[20]E. Muka, T. Mertelmeier, R. M. Slone, and E. Senol, "Impact of phosphor luminance noise on the specification of high-resolution CRT displays for medical imaging," Proc. SPIE **3031**, 210–221 (1997).
[21]E. Samei, "AAPM/RSNA Physics tutorial for residents: Technological and psychophysical considerations for digital mammographic displays," Radiographics **25**, 491–501 (2005).
[22]M. P. Eckstein, J. L. Bartroff, C. K. Abbey, J. S. Whiting, and F. O. Bochud, "Automated computer evaluation and optimization of image compression of x-ray coronary angiograms for signal known exactly detection tasks," Opt. Express **11**, 460–475 (2003).
[23]E. Samei, M. J. Flynn, and W. R. Eyler, "Detection of subtle lung nodules: Relative influence of quantum and anatomic noise on chest radiographs," Radiology **213**, 727–734 (1999).
[24]R. S. Saunders, Jr., E. Samei, and C. Hoeschen, "Impact of resolution and noise characteristics of digital radiographic detectors on the detectability of lung nodules," Med. Phys. **31**, 1603–1613 (2004).
[25]E. Samei and S. L. Wright, "Luminance and contrast performance of liquid crystal displays for mammographic applications," Technol. Cancer Res. Treat. **3**, 429–436 (2004).

A Monte Carlo Investigation on the Impact of Scattered Radiation on Mammographic Resolution and Noise

Robert S Saunders, Jr [a,b], Ehsan Samei [a,b,c]
[a] Duke Advanced Imaging Labs, Department of Radiology,
Duke University Medical Center
[b] Department of Physics, Duke University
[c] Department of Biomedical Engineering, Duke University

ABSTRACT

Scattered radiation plays a significant role in mammographic imaging, with scatter fractions over 50% for larger, denser breasts. For screen-film systems, scatter primarily affects the image contrast, reducing the conspicuity of subtle lesions. While digital systems can overcome contrast degradation, they remain susceptible to scatter's impact on the image resolution and noise. To better understand this impact, we have created a Monte Carlo model of a mammographic imaging system adaptable for different imaging situations. This model flags primary and scatter photons and therefore can produce primary-only, scatter-only, or primary plus scatter images. Resolution was assessed using the edge technique to compute the Modulation Transfer Function (MTF). The MTF of a selenium detector imaged with a 28 kVp Mo/Mo beam filtered through a 6 cm heterogeneous breast was 0.81, 0.0002, and 0.65 at 5 mm^{-1} for the primary beam, scatter-only, and primary plus scatter beam, respectively. Noise was measured from flat-field images via the noise power spectrum (NNPS). The NNPS-exposure product using the same imaging conditions was $1.5 \cdot 10^{-5}$ $mm^2 \cdot mR$, $1.6 \cdot 10^{-5}$ $mm^2 \cdot mR$, and $1.9 \cdot 10^{-5}$ $mm^2 \cdot mR$ at 5 mm^{-1} for the primary, scatter, and primary plus scatter beam, respectively. The results show that scatter led to a notable low-frequency drop in the MTF and an increased magnitude of the NNPS-exposure product. (This work was supported in part by USAMRMC W81XWH-04-1-0323.)

Keywords: Image Quality, Mammography, Simulation, Monte Carlo, Modulation Transfer Function, MTF, Noise Power Spectrum, NNPS

1. INTRODUCTION

Scattered radiation has a significant impact on image quality in medical imaging. For mammographic imaging, previous studies have estimated that 50% of all photons reaching the detector when imaging large, dense breasts are scattered photons.[1] Scatter's effects depend on the particular x-ray detector used. For screen-film detectors, scatter diminishes the conspicuity of subtle lesions by reducing the image contrast. These contrast limitations are not faced by digital mammography. Digital mammography is affected, however, by scatter's effects on image resolution and noise. To measure the magnitude of these effects, this study examines system resolution and noise with and without the presence of scatter in a variety of imaging situations. By computing scatter properties, mammography detectors can be designed to more effectively reduce the deleterious effects of scattered radiation.

2. METHODS AND MATERIALS

2.1 Monte Carlo Description

To isolate the effects of scatter and primary radiation, this study used simulation methods. It simulated the photon transport physics using Penelope Monte Carlo code (version 2005).[2] Penelope performs accurate simulation of the physical photon interactions through use of both numerical databases and analytical cross-sections. Penelope has been proven accurate for electrons, positrons, and photons in the range of 50 eV to 1 GeV.[3]

The Monte Carlo was used to form a model of a direct flat-panel mammography system. This model, as shown in Figure 1, consisted of an anode, breast phantom, and a selenium detector. For resolution studies, a tungsten edge was positioned on top of the breast in order to compute an edge spread function. In addition, for some runs an antiscatter grid was located on top of the detector to explore the effects of these devices. To ensure the realism of this model, published data was used to set the physical properties for the photons, material compositions, and attenuation. The photons were emitted from the anode according to an angular distribution based on previous work.[4] The photon energies were distributed according to previously measured bremsstrahlung distributions filtered by the tube filtration.[5-7] The molecular composition of glandular material was provided by previous publications,[8] while the composition of adipose tissue was provided by Penelope.[9] Attenuation data for all materials was provided by Penelope.

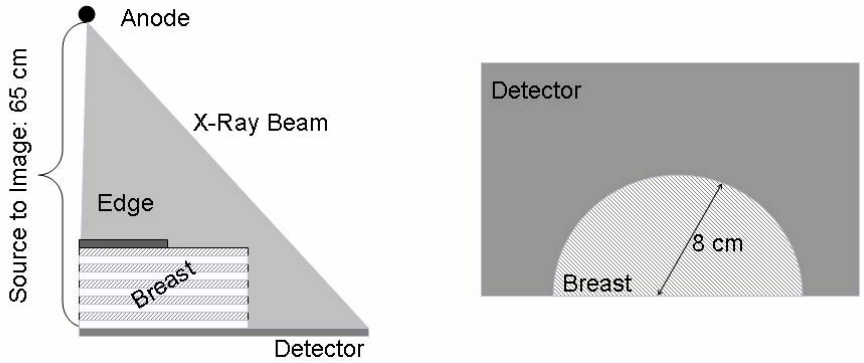

Figure 1. Schematic of simulated imaging system. In this case, the breast has a heterogeneous composition, such that the breast is composed of ten interleaving slabs of glandular and adipose tissue. The tungsten edge is used for assessing resolution, but is removed for noise evaluation.

Once a photon underwent a scattering event, such as coherent scatter or incoherent/Compton scatter, the photon was labeled as a scattered photon. Any secondary particles created from an interaction also were labeled as scattered photons. By using this labeling, the code could produce images containing only primary photons, only scattered photons, or both primary and scattered photons. If a photon interacted with the detector, the code would track the electrons produced and record the electron's position and energy. The positions were binned into pixels of 0.05 mm and the energy was integrated to produce the image signal. In addition, the code recorded the energy spectrum of all photons impinging upon the detector, regardless of whether these photons were recorded by the detector.

To efficiently investigate the effects of different model parameters, we established a default case, as shown in Table I. The effect of a specific parameter was investigated by setting all other parameters to their default value and varying only that one parameter. For instance, to explore the effects of different beam energies, all other parameters were held constant (breast composition, anode type, breast thickness, breast location, and grid status) and only the energy of the x-ray beam was varied.

Table I. Range of Simulation Parameters. The effects of specific parameters are investigated by using default values for all other parameters and varying that specific parameter.

Parameter	***Default Value***	***Range of Values***
Breast Composition	Heterogeneous	100% Adipose, Heterogeneous, 100% Glandular
Grid Status	No Grid	No Grid, Mammographic Grid
Beam Energy	28 kVp	25 kVp, 28 kVp, 32 kVp, 35 kVp
Location	Breast Center	Chest Wall, Breast Center, Nipple
Breast Thickness	6 cm	2 cm, 4 cm, 6 cm, 8 cm
Tube	Mo/Mo	Mo/Mo, W/Rh

To further model mammographic systems, all images were gain corrected to account for intensity variations. Emulating commercial systems, 10 images were acquired of a 4 cm Lucite block placed at the tube side of the system (63 cm from the detector). The 10 images were averaged together to form the gain map. All images were corrected by the appropriate gain map as:

$$I'(x,y) = \frac{\bar{G}}{G(x,y)} \cdot I(x,y) \tag{1}$$

where I represents the input image, I' corresponds to the corrected image, and G is the average of the 10 gain images with mean $\bar{G}$. There was no offset correction as the simulated system had zero offset: an image acquired at zero exposure would have zero signal everywhere.

2.2 Resolution and Noise Assessment

Resolution was assessed through the Modulation Transfer Function (MTF).[10] This was accomplished using modified versions of established assessment routines.[11-13] Briefly, the routine went through the following steps. The routine first smoothed the image with a Gaussian smoothing kernel to reduce noise and then used a Sobel method to find the edge transition. The edge angle and intercept were determined through a linear regression. However, as the edge angle was known *a priori* for these simulation studies, that parameter was entered in manually. By binning the data along lines parallel to the edge transition, the edge spread function (ESF) was computed. As opposed to previous publications, in this work the line spread function was not computed using a finite difference, as this was overly sensitive to noise. Rather, the LSF was found from a third order moving polynomial fit. After computing the polynomial fit for an area around a given point, the derivative of that fit became the value of the line spread function for that point. Figure 2 shows examples of this polynomial differentiation compared to finite difference techniques.

Figure 2. Examples of different differentiation methods without noise (left) and with modest noise (right). The top plot shows an edge spread function with its associated line spread functions underneath. Without noise, finite difference methods and the polynomial method gave similar answers (differing by 0.3% over the range from -10 mm to 10 mm). However, in the presence of moderate noise, the two methods gave dramatically different answers. The polynomial method produced a similar LSF to the case without noise, while the finite difference method produced a substantially noisier LSF in which the line peak is barely visible.

Next, the resolution assessment routine smoothed the tails of the LSF to lower the noise of the MTF while preserving the central area of the line spread function. This preserved the shape of the MTF, as the MTF shape is determined by the width of the line spread function peak, but the smoothing removed significant amounts of noise. Finally, the LSF was transformed by a Fast Fourier Transform (FFT), normalized by its value at zero frequency, and the MTF was computed as the absolute value of that quantity.

Noise was measured by the Noise Power Spectrum (NNPS).[14-16] The images were segmented into 49 overlapping ROIs that measured 6.4 mm x 6.4 mm in size. The routine subtracted off the mean of each ROI and then normalized each by their mean and the pixel size. Each ROI was scaled by the ratio of its mean to the mean of the ROI in the top-left hand corner, to minimize the influence of intensity variations across the image. Each ROI was transformed by an FFT, averaged together, and normalized to form the NNPS. Profiles of the NNPS were taken in the radial, horizontal, vertical, and axial directions by averaging a ±5 pixel wide band through the NNPS. The NNPS were then multiplied by their exposure, as the NNPS of a linear system should scale linearly with exposure. This would discriminate between situations where the NNPS is low because it was acquired at a lower dose or because the imaging parameters used led to lower noise.

3. RESULTS

Figure 2 shows the energy spectrum of the photons reaching the detector for the default simulation case (6 cm heterogeneous breast, 28 kVp, Mo/Mo tube, no grid, center of breast). Figure 3 also shows the energy spectrum of the photons reaching the detector, including both primary and scatter, for varying beam energies. For each beam energy, the photon energy spectrum appears roughly similar for photons below 20 keV, with higher energy beams showing more photons at higher energies. Table II illustrates the scatter fractions for various beam energies. Similar to previous work,[1] scatter fractions appeared roughly constant with increasing energy.

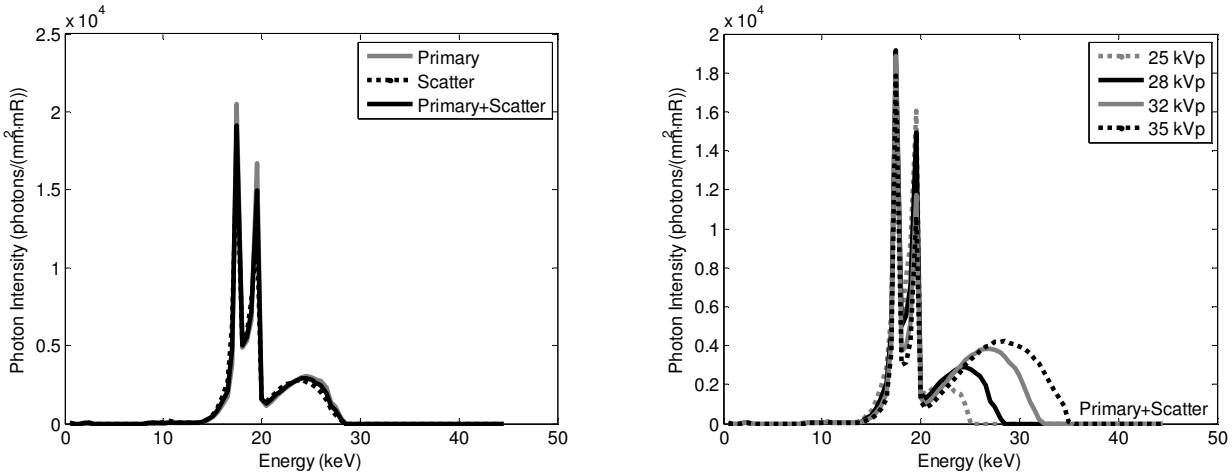

Figure 3. Normalized energy spectrum of photons, with primary-only, scatter-only, and primary plus scatter cases, reaching the detector for the default simulation case (left). Energy spectrum of all photons reaching the detector (primary plus scatter) for varying beam energies, keeping all other parameters constant (right).

Table II. Scatter fraction for various beam energies. The scatter fraction stays roughly constant with beam energy.

Beam Energy (kVp)	Scatter Fraction
25	0.387
28	0.387
32	0.386
35	0.385

Figure 4 illustrates the resolution and noise for the default simulation case. Scattered photons caused a low-frequency drop in the MTF, but also slightly changed the shape of the MTF at higher frequencies. The scattered photons act like a large blurring kernel, as indicated by its very low MTF. For the noise, scattered photons decreased the signal to noise ratio of the images, as NNPS multiplied by exposure increased between the primary-only case and the primary plus scatter case. Figure 5 shows the resolution and noise for different beam energies. The MTF and NNPS appear roughly constant across beam energies.

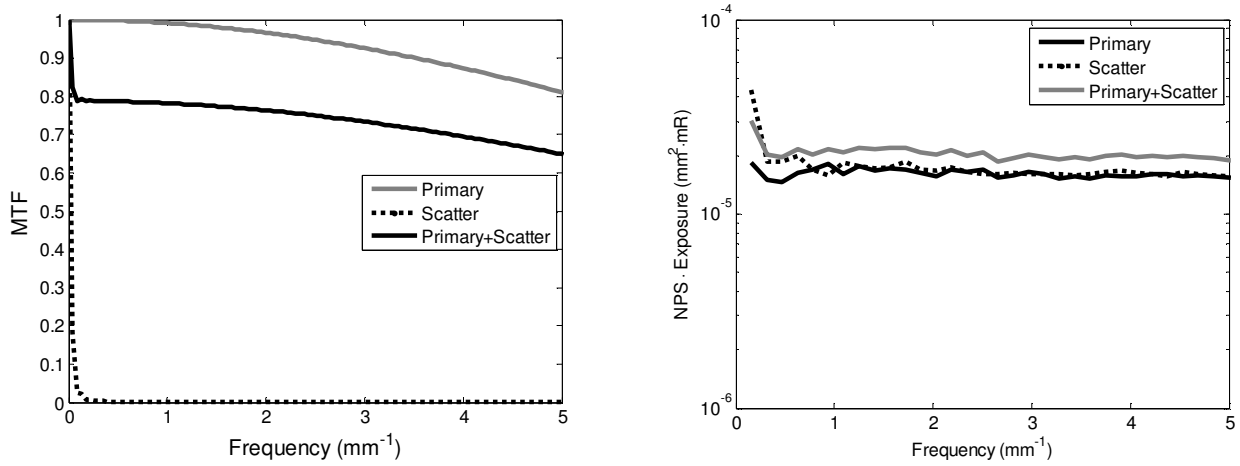

Figure 4. Resolution (left) and noise (right) for the default simulation case for primary photons only, scattered photons only, and primary plus scattered photons. Noise is represented by the radial trace of the NNPS multiplied by exposure, as the NNPS of a linear system should be inversely proportional to exposure.

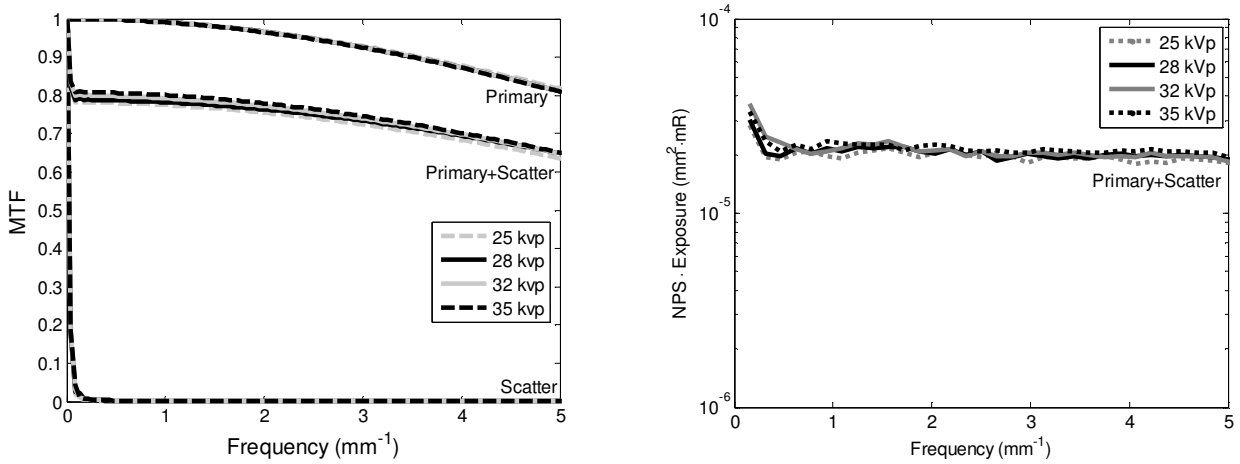

Figure 5. Resolution (left) and noise (right) for different beam energies, while controlling all other simulation parameters. The MTFs are plotted for the primary, scatter, and primary plus scatter cases, while the noise metric, the radial trace of the NNPS multiplied by exposure, only represent the noise for the primary plus scatter cases.

4. DISCUSSION AND CONCLUSIONS

Several previous investigations have modeled the scatter in radiographic systems, but have focused only on scatter fractions, contrast improvement, or signal to noise ratios.[1,17-23] A limited number of investigations have examined some aspect of the resolution and noise effects of scatter.[24-26] However, no previous work has comprehensively examined the resolution and noise effects of scattered radiation.

This study examined the resolution and noise of an imaging system both with and without the presence of the scatter. The results show how scatter affects the frequency content of images. For the MTF, scatter leads to a low-frequency drop but also changes the shape of the MTF, especially at higher frequencies. For noise, scattered photons add considerable noise to the image, leading to NNPS-exposure products with greater magnitudes.

Several items are planned for future work. The first step would be to record the glandular dose for each imaging situation. Glandular dose would allow researchers to weight the resolution and noise advantages versus the dose given to the patient. Second, the model will incorporate more scatter rejection devices, especially slot-scan devices, to expand the model utility. Finally, these results should be compared against measured results to ensure the validity of the model.

ACKNOWLEDGEMENTS

The authors wish to thank Aldo Badano and Chee Hoe for several useful conversations. This work was supported in part by USAMRMC W81XWH-04-1-0323.

REFERENCES

[1] J. M. Boone, K. K. Lindfors, V. N. Cooper, 3rd et al.,"Scatter/primary in mammography: comprehensive results," Med Phys **27**, 2408-2416 (2000).

[2] F. Salvat, J.-M. Fernandez-Varea, E. Acosta et al., *PENELOPE—A Code System for Monte Carlo Simulation of Electron and Photon Transport*. (OECD Publications, Paris, France, 2001).

[3] J. Sempau, J. M. Fernandez-Varea, E. Acosta et al.,"Experimental benchmarks of the Monte Carlo code PENELOPE," Nucl Instrum Methods B **207**, 107-123 (2003).

[4] M. R. Ay, M. Shahriari, S. Sarkar et al.,"Monte carlo simulation of x-ray spectra in diagnostic radiology and mammography using MCNP4C," Phys Med Biol **49**, 4897-4917 (2004).

[5] J. M. Boone, T. R. Fewell, and R. J. Jennings,"Molybdenum, rhodium, and tungsten anode spectral models using interpolating polynomials with application to mammography," Med Phys **24**, 1863-1874 (1997).

[6] J. Hubbell and S. M. Seltzer (2004), *Tables of X-Ray Mass Attenuation Coefficients and Mass Energy-Absorption Coefficients* [Online] Available: http://physics.nist.gov/xaamdi [January 20, 2006]. National Institute of Standards and Technology, Gaithersburg, MD

[7] J. Schweppe, X-Ray Attenuation and Energy Absorption (Wolfram Information Center, Champaign, IL, 2002).

[8] International Commission on Radiation Units and Measurements., *Tissue substitutes in radiation dosimetry and measurement*. (International Commission on Radiation Units and Measurements, Bethesda, Md., U.S.A., 1989).

[9] M. J. Berger, ESTAR, PSTAR, and ASTAR: Computer Programs for Calculating Stopping-Power and Ranges for Electrons, Protons, and Helium Ions, NIST Report NISTIR-4999,Washington, DC 1992.

[10] K. Rossmann,"Point spread-function, line spread-function, and modulation transfer function. Tools for the study of imaging systems," Radiology **93**, 257-272 (1969).

[11] R. S. Saunders and E. Samei,"A method for modifying the image quality parameters of digital radiographic images," Med Phys **30**, 3006-3017 (2003).

[12] R. S. Saunders, Jr., E. Samei, J. L. Jesneck et al.,"Physical characterization of a prototype selenium-based full field digital mammography detector," Med Phys **32**, 588-599 (2005).

[13] R. S. Saunders and E. Samei,"Resolution and noise measurements of five CRT and LCD medical displays," Med Phys **33**, 308-319 (2006).

[14] M. L. Giger, K. Doi, and H. Fujita,"Analysis of Noise Wiener Spectra in Digital Ii/Tv Imaging-Systems," Med Phys **11**, 385-385 (1984).

[15] M. L. Giger, K. Doi, and C. E. Metz,"Investigation of Basic Imaging Properties in Digital Radiography.2. Noise Wiener Spectrum," Med Phys **11**, 797-805 (1984).

[16] M. L. Giger, K. Doi, and H. Fujita,"Investigation of Basic Imaging Properties in Digital Radiography.7. Noise Wiener Spectra of II-TV Digital Imaging-Systems," Med Phys **13**, 131-138 (1986).

[17] Z. Jing, W. Huda, and J. K. Walker,"Scattered radiation in scanning slot mammography," Med Phys **25**, 1111-1117 (1998).

[18] H. P. Chan, K. L. Lam, and Y. Z. Wu,"Studies of performance of antiscatter grids in digital radiography: effect on signal-to-noise ratio," Med Phys **17**, 655-664 (1990).

[19] P. J. Papin and P. S. Rielly,"Monte Carlo simulation of diagnostic x-ray scatter," Med Phys **15**, 909-914 (1988).

[20] M. Endo, T. Tsunoo, and N. Nakamori,"Effect of scatter radiation on image noise in cone beam CT," Proc. SPIE **3977**, 514-521 (2000).

[21] G. Barnea and C. E. Dick,"Monte Carlo studies of x-ray scattering in transmission diagnostic radiology," Med Phys **13**, 490-495 (1986).

[22] H. P. Chan and K. Doi,"Some properties of photon scattering in water phantoms in diagnostic radiology," Med Phys **13**, 824-830 (1986).
[23] H. P. Chan, Y. Higashida, and K. Doi,"Performance of antiscatter grids in diagnostic radiology: experimental measurements and Monte Carlo simulation studies," Med Phys **12**, 449-454 (1985).
[24] J. M. Boone and J. A. Seibert,"Monte Carlo simulation of the scattered radiation distribution in diagnostic radiology," Med Phys **15**, 713-720 (1988).
[25] J. M. Boone and J. A. Seibert,"An analytical model of the scattered radiation distribution in diagnostic radiology," Med Phys **15**, 721-725 (1988).
[26] H. P. Chan and K. Doi,"Physical characteristics of scattered radiation in diagnostic radiology: Monte Carlo simulation studies," Med Phys **12**, 152-165 (1985).